January 1995

State-selected ion-molecule reactions: Charge transfer and atomic rearrangement processes in thermal energy collisions of H_2^+ (X;v)+N_2 and of N_2^+ (X,A;v) + H_2

Cornelis J. Uiterwaal
University of Nebraska - Lincoln, cuiterwaal2@unl.edu

J. van Eck
Utrecht University, 3508 TA Utrecht, The Netherlands

A. Niehaus
Utrecht University, 3508 TA Utrecht, The Netherlands

State-selected ion-molecule reactions: Charge transfer and atomic rearrangement processes in thermal energy collisions of $H_2^+(X;v)+N_2$ and of $N_2^+(X,A;v)+H_2$

C. J. G. J. Uiterwaal,[a] J. van Eck, and A. Niehaus
Debye Institute, Department of Atomic and Interface Physics, Utrecht University, P.O. Box 80000, 3508 TA Utrecht, The Netherlands

(Received 22 August 1994; accepted 5 October 1994)

Using the photo-electron-product-ion-coincidence method (PEPICO) we have measured state-selective cross sections for the following processes: (A) $N_2^+(X,A;v)+H_2\rightarrow N_2H^++H$, (B) $H_2^+(X;v)+N_2\rightarrow N_2H^++H$, (C) $N_2^+(X,A;v)+H_2\rightarrow H_2^++N_2$, and (D) $H_2^+(X;v)+N_2\rightarrow N_2^++H_2$. The measurements were performed at thermal velocities ($E_{\text{c.m.}}\approx 40$ meV). We have found that the charge transfer processes (C) and (D) have cross sections that are at least an order of magnitude smaller than the cross sections for the rearrangement processes (A) and (B). The cross section for reaction (A) with $N_2^+(A;v)$ as reactant is found to be $(50.2\pm 2.4)\%$ of the cross section for the same reaction with $N_2^+(X;v)$ as reactant. The cross section for reaction (B) is found to be independent of the internal energy of the reactant ion. The measured variation of the cross sections as a function of the internal energy of the reacting ion is compared with calculations based on a RRKM type statistical model and an electronic correlation diagram of the $(N_2–H_2)^+$ system. Excellent agreement is found, indicating complete randomization of internal energy within the collision complex. Absolute cross sections are determined for the rearrangement reactions: for reaction (A) the cross section is 76.1 Å^2 starting with $N_2^+(X;v=0,1)$ and 38.05 Å^2 starting with $N_2^+(A;v=0–5)$. For reaction (B) the cross section is 114 Å^2 for $H_2^+(X;v=0–6)$. © *1995 American Institute of Physics.*

I. INTRODUCTION

In this paper, we will discuss measurements on the following ion–molecule reactions and charge transfer processes:

$$N_2^+(X,A;v)+H_2\rightarrow N_2H^++H \quad (Q=-2.535 \text{ eV}), \tag{1}$$

$$N_2^+(X,A;v)+H_2\rightarrow H_2^++N_2 \quad (Q=-0.155 \text{ eV}), \tag{2}$$

and

$$H_2^+(X;v)+N_2\rightarrow N_2H^++H \quad (Q=-2.380 \text{ eV}), \tag{3}$$

$$H_2^+(X;v)+N_2\rightarrow N_2^++H_2 \quad (Q=+0.155 \text{ eV}), \tag{4}$$

where Q denotes the heat of reaction (positive sign for endothermal reactions). Our measurements were performed under thermal conditions with $E_{\text{c.m.}}\approx 40$ meV.

In the present experiments the nitrogen reactant ion was initially produced in three electronic states: $N_2^+(X\ ^2\Sigma_g^+)$, $N_2^+(A\ ^2\Pi_u)$, and $N_2^+(B\ ^2\Sigma_u^+)$, for several values of the vibrational quantum number v. The ground state electronic configuration of the neutral nitrogen molecule $N_2(X\ ^1\Sigma_g^+)$ is given by $(\sigma_g1s)^2(\sigma_u1s)^2(\sigma_g2s)^2(\sigma_u2s)^2(\pi_u2p)^4(\sigma_g2p)^2$. Writing N_2 for this electronic configuration, the electronic configurations of the three produced electronic states of the ion can be written as (giving only the dominant components):[1,2] $N_2^+(X\ ^2\Sigma_g^+)=N_2(\sigma_g2p)^{-1}$ and $N_2^+(A\ ^2\Pi_u)=N_2(\pi_u2p)^{-1}$; the third state, $N_2^+(B\ ^2\Sigma_u^+)$, has two dominant components, namely $N_2(\sigma_u2s)^{-1}$ and $N_2(\pi_u2p)^{-1}(\sigma_g2p)^{-1}(\pi_g2p)^1$. Both $N_2^+(A\ ^2\Pi_u)$ and $N_2^+(B\ ^2\Sigma_u^+)$ decay radiatively to $N_2^+(X\ ^2\Sigma_g^+)$; in the case of $N_2^+(B\ ^2\Sigma_u^+)$ this decay is too fast[2] ($\tau=6.25\times10^{-8}$ s) to allow measurements of the reactivity of this electronic state. Radiative decay will be discussed in Sec. III B. The hydrogen ion was produced exclusively in the electronic ground state $H_2^+(X\ ^2\Sigma_g^+)$, in several vibrational states.

Anderson *et al.*[3] studied processes (3) and (4) using a method combining photoionization and a radio frequency guided ion technique. They investigated reactions involving the states $H_2^+(X;v=0–4)$. The center of mass energies $E_{\text{c.m.}}$ in their experiments ranged from 0.5 to 9 eV. They found that at low energies, the reactive process (3) ''appears to be dominated by a mechanism which is relatively independent of vibrational state.'' Their measurements clearly show that in collisions of $H_2^++N_2$, proton transfer [process (3)] starts dominating more and more over charge transfer [process (4)] as the collision energy is lowered.

Henri *et al.*[4] used a TPEPICO (threshold-photoelectron-product-ion-coincidence) technique using synchrotron radiation to measure cross sections for process (2) for $E_{\text{c.m.}}=0.70$ and 0.97 eV, for $N_2^+(X;v=0–4)$ and for $N_2^+(A;v=0–5)$. They found a weak dependence on the vibrational level. They determined absolute cross sections, and concluded that the charge transfer cross section behaves like $\sigma_{\text{CT}}=aE_{\text{c.m.}}$, with $a=9.0$ Å^2/eV. At these center of mass energies of 0.70 and 0.97 eV, they expected N_2H^++H to be the major product channel. This was confirmed by a comparison of their results with measurements of absolute cross sections for this reactive channel done by Hierl *et al.*[5] at approximately the same center of mass energies. Henri *et al.* also

[a]Present address: FORTH-IESL, P.O. Box 1527, 71110 Heraklion, Crete, Greece.

 0021-9606/95/102(2)/744/10/$6.00

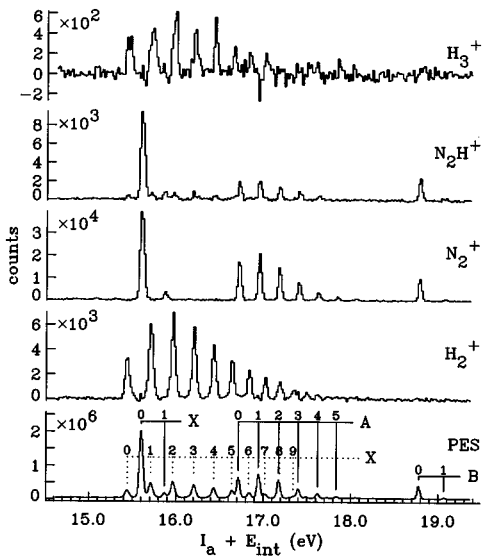

Fig. 1. Measured coincident ion spectra. The horizontal axis shows the adiabatic ionization potential I_a plus the internal energy E_{int} of the ion. The zero of energy is chosen to coincide with H_2+N_2, both in their ground states. The bottom spectrum is the HeI photoelectron spectrum (PES) of the mixture of H_2 and N_2. In this spectrum, the peaks corresponding to $N_2^+(X;v=0,1)$, $N_2^+(A;v=0,1,2,3,4,5)$, and $N_2^+(B;v=0,1)$ are indicated using solid lines. The other peaks, indicated with dotted lines, are from $H_2^+(X;v)$. The upper four spectra show the number of ions counted in coincidence with a photoelectron. These ion spectra were obtained by subtracting an uncorrelated ion signal (extraction of the ions 100 μs after detection of the photoelectron) from a correlated signal (extraction of the ions 1 μs after detection of the photoelectron). From bottom to top the following ion spectra are shown: $H_2^+(M=2)$, $N_2^+(M=28)$, $N_2H^+(M=29)$, and $H_3^+(M=3)$.

measured total cross sections for processes (3) and (4) together,[6] for $H_2^+(X;v=0,1,2)$ at $E_{\text{c.m.}}=9.3$ eV. At this energy, a strong vibrational dependence was found.

Schultz *et al.*[7] studied reactions (1) and (2) using guided-ion beam mass spectrometry. They worked with $N_2^+(X;v=0)$ exclusively, and with center of mass energies in the range 6 meV $\leqslant E_{\text{c.m.}} \leqslant$10 eV. They found charge transfer, reaction (2), to be of minor importance, occurring with a cross section <1 Å^2. For H atom transfer, reaction (1), they found a cross section comparable to the Langevin cross section at their lowest energies, but above about 10 meV they observed a cross section that is somewhat larger than the Langevin cross section. This was attributed to the occurrence of charge transfer before the formation of N_2H^+.

Tosi *et al.*[8] studied reaction (1) (plus its analog with D_2 as the neutral reactant) using a crossed beam apparatus. The distribution over internal energies in their experiment was 90% $N_2^+(X;v=0)$ and 10% $N_2^+(X;v\geqslant 1)$. Center of mass energies were in the range 25 meV $\leqslant E_{\text{c.m.}} \leqslant$2 eV. They observed structures in the energy dependence of the cross sections for both reactions, that they attributed to the opening of reactive channels in an intermediate charge transfer complex.

Koyano *et al.*[9] used a threshold-electron-secondary-ion-coincidence (TESICO) technique to study reactions (1) and (2) using D_2 instead of H_2 at $E_{\text{c.m.}}=1.3$ eV. They also studied reactions (3) and (4) using H_2^+, HD^+, and D_2^+ at $E_{\text{c.m.}}=2.5$ eV. They concluded that, at these energies, reaction (1) proceeds via a nonadiabatic transition to the $D_2^+ + N_2$ surface. However, the detailed mechanism is not clear.

TABLE I. Radiative lifetimes $\tau_{v'}$ of $N_2^+(A;v')$ decaying to $N_2^+(X;v'')$ for values of v' relevant to this work. Values taken from Ref. 20.

v'	0	1	2	3	4	5
$\tau_{v'}(\mu s)$	16.6	13.9	12.0	10.7	9.68	8.89

To our knowledge, the group of Koyano *et al.* is the only one that has performed measurements on the atomic rearrangement reaction (1) for $N_2^+(A;v)$, and the present work is the first to include measurements on this reaction for $N_2^+(A;v)$ using thermal collision energies.

II. EXPERIMENT

The experiments described in this paper were carried out using the PEPICO (photo-electron-product-ion-coincidence) apparatus described earlier.[10–13] The main parts of the apparatus are a HeI resonance lamp, a cylindrical mirror electron analyzer (CMA) and a time-of-flight (TOF) ion mass spectrometer of the reflectron type[13] (simply called "reflectron" here), replacing the more simple type of ion mass spectrometer described in Refs. 10–12. In the heart of the apparatus a mixture of H_2 and N_2 gas enters into a gas chamber through a circular slit. We used commercially available gases, both having purity better than 99.99%. Inside the chamber, the gas is irradiated with vacuum ultraviolet (VUV) radiation produced in the lamp ($h\nu=21.22$ eV), and primary (i.e., reactant) ions are formed through photoionization. The internal energy of the primary ions is determined by measuring the kinetic energy E_{kin} of the ejected photoelectrons with the CMA. The energy resolution of the CMA ranges from $\Delta E/E\approx 1\%$ for $E_{\text{kin}}=2$ eV to $\Delta E/E\approx 0.7\%$ for $E_{\text{kin}}=10$ eV. After their transition through the CMA, the photoelectrons are detected using a channeltron. The photoionization chamber serves as reaction chamber at the same time. The primary ions remain in the chamber under strictly field-free conditions for a fixed time span of 1 μs, the so-called reaction time span. This gives the primary ions the possibility to collide with a neutral gas particle and react, thus forming secondary (i.e., product) ions. The gas pressures are chosen low enough to guarantee single-collision conditions to a good approximation, i.e., a reaction probability of no more than about 10%. The electron detection signal starts a pulsed time-of-flight measurement after passing through two delays, one compensating for different transit times through the CMA of photoelectrons with different kinetic energies, and the other fixing the reaction time span to the chosen value. After passing through these two delays, the signal triggers a negative voltage, extracting all ions present in the reaction chamber (reactant as well as product ions) and bringing them into the reflectron. Inside the reflectron, the ions pass through an acceleration region, a deflector, a drift region, a reflecting section, and a drift region again, and finally they are detected

using a two-stage array of micro-channel plates. The resolution of our reflectron is $M/\Delta M \approx 300$. The ions that are detected using the measuring protocol just described form the so-called correlated coincident spectrum. To correct for random coincidences, an uncorrelated coincident spectrum is measured as well. It is obtained by delaying the detection signal of every second electron detected by the channeltron for an extra time of 100 μs before applying the extraction voltage pulse. Random coincidences are removed from the correlated coincident spectrum by subtracting the uncorrelated coincident spectrum from it, thus producing a net coincident spectrum containing the physical information. Four different masses can be detected and counted in one experiment by putting appropriate windows in the resulting TOF spectrum. The experiment is controlled by a PDP 11/23 computer, which also stores the data and sends them to the central laboratory DEC 4000 server, where they are processed subsequently.

III. MEASURED REACTION CROSS SECTIONS

A. General

The measured spectra (random coincidences subtracted) are shown in Fig. 1. To record the spectra, the transmission energy of the CMA electron spectrometer was scanned 35140 times over the range 1.86 eV$\leqslant E_{\rm kin} \leqslant$6.59 eV, where $E_{\rm kin}$ denotes the kinetic energy of the photoelectron. Each scan consists of 512 equal steps (or channels). Between two successive steps, the transmission energy is kept constant for 100 ms. The total data collection time per channel is 3514 s. The pressure in the reaction chamber of both H_2 and N_2 is estimated to be $\sim 10^{-2}$ Pa (or $\sim 10^{-4}$ Torr). Pressure dependent measurements showed that these pressures are low enough to assure single collision conditions. The bottom figure shows the photoelectron spectrum (PES). In this spectrum, three bands of molecular nitrogen are indicated corresponding to the $N_2^+(X)$, $N_2^+(A)$, and $N_2^+(B)$ electronic state. The vibrational quantum numbers are indicated in the figure. The other band (indicated using dotted lines) corresponds to $H_2^+(X)$. The energy axis shows the adiabatic ionization potential[14] I_a plus the internal energy $E_{\rm int}$ of the ion, given by

$$h\nu - E_{\rm kin} = I_a + E_{\rm int}, \tag{5}$$

where $h\nu = 21.22$ eV is the energy of the HeI $2^1P \rightarrow 1^1S$ photon. The energy axis was calibrated using the known[15] adiabatic ionization potentials of $N_2^+(X;v=0)$ at $I_a = 15.60$ eV and of $N_2^+(B;v=0)$ at $I_a = 18.78$ eV. Coincidence spectra were recorded for four different masses: $H_2^+(M=2)$, $N_2^+(M=28)$, $N_2H^+(M=29)$, and $H_3^+(M=3)$. No other masses were observed in the time-of-flight spectrum. The H_3^+ ions are formed in the reaction[16] $H_2^+(X;v) + H_2 \rightarrow H_3^+ + H$. The occurrence of this reaction does not influence our present measurements on reactions (1)–(4).[17]

As Fig. 1 shows, the photoelectron spectra of H_2 and N_2 are almost free of overlap, allowing us to identify the reactant ion unambiguously in most cases. To obtain internal energy dependent relative cross sections σ from these spectra, we divided the energy axis into several regions, each corresponding to a complete peak of N_2^+ or H_2^+, and determined the contents of these regions for each spectrum. For each energy region, σ (in arbitrary units) is then given by the fraction

$$\sigma = \frac{[\text{product ions}]}{[\text{product ions}] + [\text{reactant ions}]}, \tag{6}$$

where the brackets denote the contents of the region. If a peak is partially overlapped by another peak, we took the nonoverlapped part of it to represent the whole peak. The standard deviation in σ is determined from the standard deviations in the contents of the regions, which in turn are determined from the Poisson standard deviations in the correlated and the uncorrelated spectra.

B. Radiative decay of $N_2^+(A)$ and $N_2^+(B)$

The electronically excited $N_2^+(A)$ and $N_2^+(B)$ states of the nitrogen molecular ion decay radiatively to the $N_2^+(X)$ state. This loss mechanism for electronically excited ions is in competition with reaction of these ions, which is the main subject of our present investigations. We must carefully study this competition to see if corrections have to be made to the observed spectra. (See also Ref. 18.)

The $N_2^+(A;v')$ ions[19] decay radiatively to $N_2^+(X;v'')$. The (v',v'')-dependent Franck–Condon factors $F_{v',v''}$ and the v'-dependent lifetimes $\tau_{v'}$ of this decay are given by Refs. 2 and 20. For convenience, the lifetimes are reproduced in Table I. To estimate the influence of radiative decay on the observed spectra, we must realize that in the experiment the time between the photoionization event and the extraction of the ions from the reaction chamber was fixed to $t_{\rm react} = 1$ μs. If the only loss mechanism for the $N_2^+(A;v')$ ions would be radiative decay, the probability of finding an $N_2^+(A;v')$ ion still surviving after a time t would be $\exp(-t/\tau_{v'})$. The mean fraction of nondecayed $N_2^+(A;v')$ ions present in the reaction chamber in the time span $0 \leqslant t \leqslant t_{\rm react}$ (the reaction time span) equals

$$P(\tau_{v'}) = \frac{\tau_{v'}}{t_{\rm react}} \{1 - \exp(-t_{\rm react}/\tau_{v'})\} \approx 1 - \frac{t_{\rm react}}{2\tau_{v'}}. \tag{7}$$

Substituting the values of $\tau_{v'}$ from Table I, we calculate that in our experimental context the probability for an $N_2^+(A;v')$ ion to react without decaying first varies from 95% (for $v'=5$) to 97% (for $v'=0$). The remaining fraction $1 - P(\tau_{v'})$ of the ions will first decay to some $N_2^+(X;v'')$ state before a reaction takes place. The experimentally observed cross section $\sigma_{\rm exp}(A;v')$ will thus be slightly different from the actual cross section $\sigma_{\rm act}(A;v')$, the ratio being given by

$$\frac{\sigma_{\rm exp}(A;v')}{\sigma_{\rm act}(A;v')} = \frac{P(\tau_{v'})\ \sigma_{\rm act}(A;v') + (1-P(\tau_{v'}))\ \Sigma_{v''} F_{v',v''}\ \sigma_{\rm act}(X;v'')}{\sigma_{\rm act}(A;v')}\ . \tag{8}$$

The summation in Eq. (8) is taken over all $N_2^+(X;v'')$ states populated by decay from $N_2^+(A;v')$, with the Franck–Condon factors as weights. To estimate the error introduced by the radiative decay, we need to know $\sigma_{\rm act}(X;v'')$ for all values of v'' encountered in Eq. (8). Since we lack this information for $v'' \geqslant 2$ we will assume that $\sigma_{\rm act}(X;v'')$ is comparable to the experimentally observed $\sigma_{\rm act}(X;v''=0,1)$ for all values of v''. We measured (see Sec. III D below) that the reaction cross section for $N_2^+(X)$ is larger than that for $N_2^+(A)$ by a factor of 1.99 ± 0.09. Taking this factor equal to 2 and substituting, we calculate for the error introduced by radiative decay

$$\frac{\sigma_{\rm exp}(A;v')}{\sigma_{\rm act}(A;v')} = P(\tau_{v'}) + 2(1-P(\tau_{v'})) = 2 - P(\tau_{v'}). \tag{9}$$

Taking the fastest decaying $v'=5$ as a (worst case) example, we see that in the experimental spectra, the cross section for reaction will be overestimated by at most 5%. Since this overestimation is relatively minor, we will neglect it in the discussion below.

The $N_2^+(B)$ state also decays radiatively. However, the lifetime of the $N_2^+(B)$ state is only 6.25×10^{-8} s (see Ref. 2, where Franck–Condon factors are also given), so that effectively all $N_2^+(B)$ state ions decay to the $N_2^+(X)$ state before reaction occurs. The internal energy of the resulting $N_2^+(X)$ ions is spread out over a range determined by the Franck-Condon factors, with the mean internal energy *after* radiative decay of an $N_2^+(B;v')$ ion given by

$$E_{\rm int,av}(B;v') = \sum_{v''} F_{v',v''} E_{\rm int}(X;v''). \tag{10}$$

The Franck–Condon factors $F_{v',v''}$ for $(B;v') \rightarrow (X;v'')$ decay are large for $v'' \approx v'$ and fall off rapidly for increasing v'' (with $|v''-v'| \leqslant 1$ for more than 80% of the ions), so that the resulting internal energy distributions are well characterized by their mean values, given by

$$\begin{aligned} E_{\rm int,av}(B;v=0) &= 0.128\ \text{eV}, \\ E_{\rm int,av}(B;v=1) &= 0.398\ \text{eV}, \end{aligned} \tag{11}$$

where the zero of energy is chosen to coincide with $N_2^+(X;0)$. For a correct interpretation, we will plot the datapoints for $N_2^+(B;v=0)$ and $N_2^+(B;v=1)$ at the energy values given by (11).

C. Charge transfer

Charge transfer should be visible in the measured spectra as an N_2^+ ion measured in coincidence with an electron corresponding to an H_2^+ ion or *vice versa*. Since most of the detected H_2^+ and N_2^+ ions are produced by direct photoionization, we will have to blow up the spectra to observe possible charge transfer. Blowing up the spectra reveals two weak phenomena that have nothing to do with charge transfer processes: (i) direct ionization caused by a small (about 4%) contribution in our VUV beam of 23.09 eV HeI $3^1P \rightarrow 1^1S$ radiation and (ii) direct 21.22 eV ionization to states with small Franck–Condon factors. We will find that both effects affect mostly the N_2^+ spectrum, because of the different structures of the HeI 21.22 eV photoelectron spectra of H_2^+ and N_2^+.

We will use Fig. 2 to discuss charge transfer. This figure shows the same data as Fig. 1, but the spectra of H_2^+, N_2^+, and N_2H^+ have been enlarged to reveal low-intensity features and to compare them on the same scale. In the ion spectra of Fig. 2, the zero level is indicated by a horizontal solid line. For the N_2^+ spectrum, the experimental error is shown as a vertical bar for each channel.

1. $H_2^+ + N_2 \rightarrow N_2^+ + H_2$

We are especially interested in the region of the N_2^+ spectrum coincident with photoelectrons from $H_2^+(X;v=0,1,2,3,4,5)$, since these hydrogen peaks are more or less separated from nitrogen peaks. In the blown-up spectra, the very weak $N_2^+(X;2)$ and $N_2^+(X;3)$ direct ionization peaks are clearly visible in this region (indicated by arrows in the figure). To get an idea of the noise level in the N_2^+ spectrum, we look at the region of this spectrum that is at the left of the $H_2^+(X;0)$ peak, where the HeI 21.22 eV PES is empty. However, we observed a small structure in this region (just visible in Fig. 1, not present anymore in Fig. 2, see below), due to $N_2^+(A;0,1,2,3)$ 23.09 eV direct ionization. The enlarged PES (dotted curve) in Fig. 2 also reveals this 23.09 eV spectrum, with peaks corresponding to $N_2^+(A;0,1,2)$ indicated by arrows. In the blown-up N_2^+ spectrum the 23.09 eV contribution has already been removed, so that the leftmost part of it now gives a correct idea of the noise in the spectrum.

To get insight in the charge transfer contribution, we will concentrate on the region coincident with $H_2^+(X;0)$ and $H_2^+(X;2)$ electrons. In these regions of the blown-up N_2^+ spectrum, we see no structure, some channels even having negative counts (which can be found because the spectra are obtained by subtraction of two measured spectra, as explained in Sec. II). For $H_2^+(X;1)$ the $N_2^+(X;0)$ direct ionization peak is very close, but in the nonoverlapped part again zero and negative counts are obtained in some channels. For $H_2^+(X;3)$, $H_2^+(X;4)$, $H_2^+(X;5)$, and $H_2^+(X;6)$ it seems that some coincident counts can be seen. However, we do not believe this to be due to charge transfer processes, because the noise level in the spectrum is substantial. For the $H_2^+(X;7)$ peak, located between $N_2^+(A;1)$ and $N_2^+(A;2)$, some significantly nonzero counts are observed, but this is the case for the whole energy range between $N_2^+(A;1)$ and $N_2^+(A;2)$, even where the $H_2^+(X;6)$ intensity drops to zero, which makes it doubtful to consider them as caused by charge transfer.

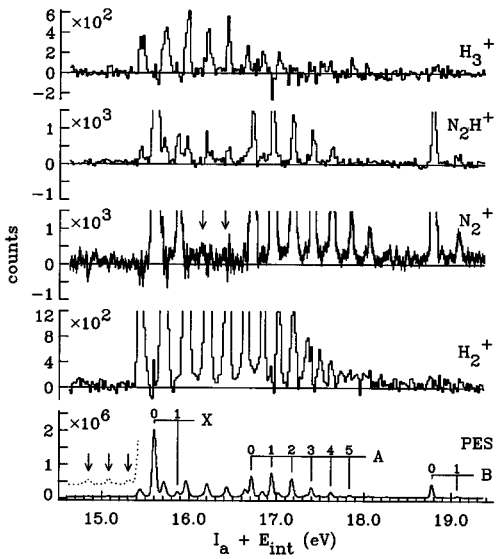

FIG. 2. Blown up coincident ion spectra. The same data as in Fig. 1 is shown here again, but now the spectra of H_2^+, N_2^+, and N_2H^+ have been blown up to see possible charge transfer products, and to compare them on the same scale. For the N_2^+ spectrum, the experimental error is shown as a vertical bar for each channel. The two arrows in this N_2^+ spectrum indicate the weak $N_2^+(X;2,3)$ direct ionization peaks. The leftmost part of the PES (bottom spectrum) is shown ten times enlarged (dotted line), revealing a very weak 23.09 eV component in the VUV emitted by our source. The three arrows here indicate electrons corresponding to N_2^+ $(A;0,1,2)$ formed by 23.09 eV photons.

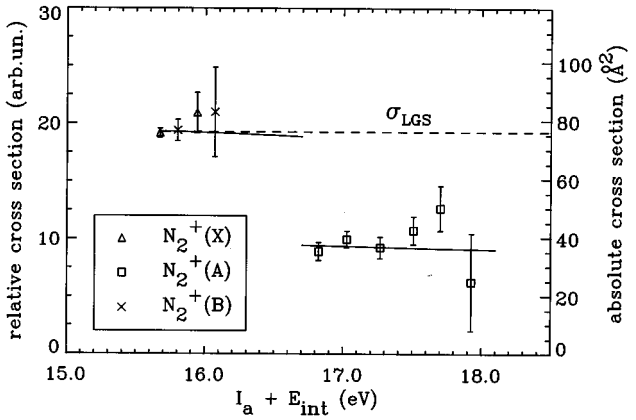

FIG. 3. Measured relative reaction cross sections for reaction (1): $N_2+H_2\rightarrow N_2H^++H$, for $N_2^+(X;v=1,1)(\triangle)$, $N_2^+(A,v=0,1,2,3,4,5)$ $(\square)$, and $N_2^+(B;v=0,1)(\times)$ (left hand vertical axis). The two points corresponding to $N_2^+(B)$ are displayed at a shifted energy to account for radiative decay, as discussed in the text. The solid curves plus the right hand vertical axis are the result of theoretical calculations producing absolute cross sections.

For comparison, the N_2H^+ coincident spectrum is shown on the same scale. Comparing the relative peak intensities of the N_2^+ and the N_2H^+ spectra, we conclude that charge transfer according to Eq. (4) has a cross section that is at least about one order of magnitude smaller than the cross section for formation of N_2H^+ for $H_2^+(X;v=0,1,2,3,4,5)$. For $H_2^+(X;v=0)$ charge transfer is endothermal and therefore a zero cross section is expected. We conclude that our measurements are in qualitative agreement with the results of Anderson *et al.*[3] (see Sec. I). Their measurements show that when the collision energy is decreased from $E_{\text{c.m.}}=9$ to 0.5 eV, initially charge transfer collisions of $H_2^+(X;v=0,1,2,3,4)+N_2$ are dominating over reactive collisions. Below about 3 eV the situation is reversed and reactive collisions start to dominate. (At their lowest energy of 0.5 eV, the cross section for reactive collisions is between 2.5 and 11 times larger than the charge transfer cross section, depending on the vibrational state.) Our measurements show that this propensity for rearrangement compared to charge transfer also occurs at $E_{\text{c.m.}}=40$ meV.

2. $N_2^+ + H_2 \rightarrow H_2^+ + N_2$

From the relative intensities of the photoelectron spectra and the coincident ion spectra it can be deduced that the ion detection efficiencies of H_2^+ and N_2^+ only differ by a factor of less than 2. We do not see any contribution from charge transfer in the H_2^+ spectrum from $N_2^+(X;0)$, the largest peak in the N_2^+ PES. For $N_2^+(A;v=0,1)$ and $N_2^+(B;v=0)$ maybe some counts are found, but comparing the spectra of H_2^+ and N_2H^+, we find that the cross section for the charge transfer process (2) is at least one order of magnitude smaller than the cross section for formation of N_2H^+ for $N_2^+(X;v=0)$, $N_2^+(A;v=0,1)$, and $N_2^+(B;v=0)$. The peaks of other states are either overlapping partially or completely with a H_2^+ state. Our conclusion that charge transfer has a cross section that is more than an order of magnitude smaller than the cross section for formation of N_2H^+ is in qualitative agreement with the work of Henri *et al.*[4] and that of Hierl *et al.*[5] (see Sec. I). From their work it follows that for $E_{\text{c.m.}}=0.97$ eV, the cross section for formation of N_2H^+ is 2.3 times larger than the charge transfer cross section. For $E_{\text{c.m.}}=0.70$ this ratio increases to 4.8. This increasing propensity for rearrangement compared to charge transfer for decreasing collision energy is confirmed by our measurements, where a ratio of at least 10 is observed.

D. Atomic rearrangement

1. $N_2^+ + H_2 \rightarrow N_2H^+ + H$

Figure 3 shows the measured relative cross sections[21] for reaction (1). As explained in Sec. III B, we display the datapoints for $N_2^+(B;v=0,1)$ at the shifted energy values given by Eq. (11) to account for $N_2^+(B;v'=0,1)\rightarrow N_2^+(X;v'')$ radiative decay. The experimentally observed cross sections for $N_2^+(X;v=0,1)$ and those observed for $N_2^+(B;v=0,1)$ are seen to be comparable, as expected because comparable internal energies are involved. The weighted means $\langle\sigma_X\rangle$ and $\langle\sigma_A\rangle$ of the four $N_2^+(X)$ and the six $N_2^+(A)$ datapoints, respectively, are $\langle\sigma_X\rangle=19.28\pm0.37$ arb.un. and $\langle\sigma_A\rangle=9.67\pm0.42$ arb.un., both in the same arbitrary units, and the ratio of the two mean reaction cross sections is given by

$$\frac{\langle\sigma_A\rangle}{\langle\sigma_X\rangle}=0.502\pm0.024. \tag{12}$$

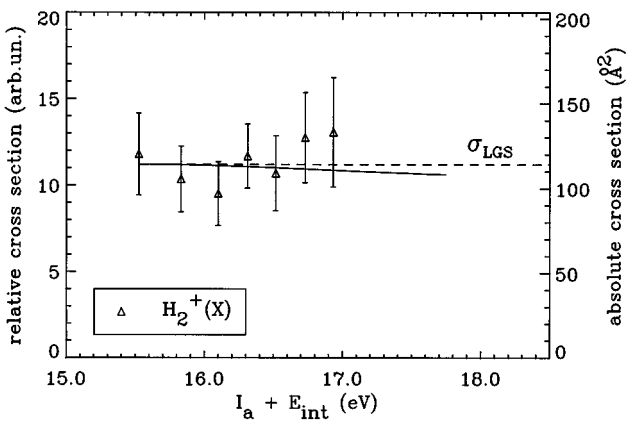

FIG. 4. Measured relative reaction cross sections for reaction (3): $H_2^+N_2 \rightarrow N_2H^+ + H$, for $H_2^+(X;v=0,1,2,3,4,5,6)$ (left hand vertical axis). Note that this figure has the same horizontal scale as Fig. 3. The solid curve plus the right hand vertical axis are the result of theoretical calculations producing absolute cross sections.

2. $H_2^+ + N_2 \rightarrow N_2H^+ + H$

Figure 4 shows the measured cross sections[21] for reaction (3). This figure has the same horizontal scale as Fig. 3. As Fig. 4 clearly shows, the cross section for reaction (3) is insensitive to the internal energy of the reactant $H_2^+(X;v)$, in contrast to the observed cross section for reaction (1). Anderson *et al.*[3] also found that reaction (3) is almost independent of vibrational energy for low collision energies (see Sec. I). The mean value of the reaction cross section equals 11.08 ± 0.82 arb.un.

IV. THEORETICAL MODEL

To explain the measured results, we performed calculations using a RRKM type theoretical model. Detailed descriptions of RRKM theory can be found in several texts.[22–24] The calculations were done using a FORTRAN code, that is available from the Quantum Chemistry Program Exchange.[25] In the calculations, it is assumed that any of the four processes proceeds via the formation of an $N_2H_2^+$* intermediate complex. The formation of this complex is described by the well-known Langevin–Gioumousis–Stevenson (LGS) model.[26,27] In the context of this model, the capture cross section (or close collision cross section) σ_{LGS} for an ion (with charge q) and a neutral molecule (with polarizability α) interacting through a $-\alpha q^2/(2R^4)$ ion-induced dipole potential is given by

$$\sigma_{\mathrm{LGS}} = \pi q \left(\frac{2\alpha}{E_{\mathrm{kin}}} \right)^{1/2}, \tag{13}$$

where E_{kin} is the asymptotic kinetic energy in the center-of-mass system. In RRKM theory, the energy available to the complex is assumed to randomize rapidly over all degrees of freedom. Also, the overall reaction rate is assumed to be controlled by the passage through a ''bottleneck'' or transition state. These two assumptions allow the probability for decay of the complex into some product channel j to be written as

$$P_j = \frac{W_j^{\ddagger}/S_j}{\Sigma_i W_i^{\ddagger}/S_i}, \tag{14}$$

where $W_j^{\ddagger}$ is the sum of states available in the transition state configuration corresponding to product channel j with energy less than or equal to the total energy available. The quantity S_j is the symmetry number for channel j. (The QCPE program calculates sums of states without considering symmetry. Therefore, symmetry must be explicitly accounted for by the factor S_j. Below, we will also use the symbol $\tilde{W}_j^{\ddagger}$ to denote the symmetry adapted sum of states for channel j, defined by $\tilde{W}_j^{\ddagger} = W_j^{\ddagger}/S_j$. A clarifying discussion of symmetry and its effects on the reaction probability is given in Ref. 24.) In the present work, the transition states of all channels are assumed to be ''loose'' transition states, i.e., they are located at the top of the centrifugal barrier that arises at rather large distances as a result of the competition between the attractive $-\alpha q^2/(2R^4)$ ion-induced dipole interaction and the repulsive $L^2/(2\mu R^2) = E_{\mathrm{kin}}(b^2/R^2)$ interaction caused by the centrifugal force (L = total angular momentum, b = impact parameter). For thermal collision energies, internal energy is not influencing the capture cross section, because the capture already takes place at a distance of typically 10 bohr, which is much larger than the typical size of the reactants. Also, because of the randomization of energy, the intermediate complex will not ''remember'' the way it was energized. As a consequence, the two processes, formation of the complex plus its subsequent decay into products, can be considered as independent processes, related only through the conservation of total energy and total angular momentum. This implies that the cross section for reaction into channel j can be expressed as[28]

$$\sigma_j(E) = \int_{\mathrm{all}\ J} dJ \, \frac{\partial \sigma_X(E,J)}{\partial J} \, P_j(E,J), \tag{15}$$

where $\partial \sigma_X(E,J)/\partial J$ is the partial close collision cross section to form a complex with energy E and angular momentum J from the reactants. Making the usual assumption that the orbital angular momentum of the collision is much larger than the internal rotational angular momenta of the separated reactant molecules, this partial close collision cross section can be written as[28]

$$\frac{\partial \sigma_X(E,J)}{\partial J} = \begin{cases} \dfrac{\pi}{\mu E_{\mathrm{kin}}} J & \text{if } J \leqslant L^* \\ 0 & \text{otherwise,} \end{cases} \tag{16}$$

where μ is the reduced mass of the two reactants and L^* is the maximum orbital angular momentum given by

$$L^* = (8\alpha q^2 \mu^2 E_{\mathrm{kin}})^{1/4}. \tag{17}$$

In the calculations, three channels were taken into account, labeled as follows: (1) $N_2^+ + H_2$, (2) $H_2^+ + N_2$, and (3) $N_2H^+ + H$. Using these labels, the probabilities of decay of the complex (having total energy E and angular momentum J) into products for processes (1)–(4) are given by

TABLE II. Parameters used in our RRKM calculations. Three channels were considered, indicated in the leftmost column, together with a characterization of the moment of inertia (spherical, linear, or atomic) of the two constituents of the channel. In the table, Q is the heat of formation with respect to $N_2^+(X;v=0)+H_2$, μ is the reduced mass of the channel, α is the polarizability of the neutral particle, ω is the set of vibrational constants of the channel, B is the set of rotational constants of the channel, and S is the rotational symmetry number of the channel. Finally, the rightmost column shows the close collision cross section σ_{LGS} for the channel, calculated using Eq. (13) with $E_{\mathrm{kin}}=\frac{3}{2}kT$ and $T=300$ K.

Channel (pair type)	Q [a] (eV)	μ (amu)	α (Å ^{3})	ω [b] (cm^{-1})	B [b] (cm^{-1})	S	σ_{LGS} (Å ^{2})
1. $N_2^+ + H_2$ (linear-linear)	0	1.87	0.79	2207 4401.21	1.93176 60.8530	4	76.1
2. $H_2^+ + N_2$ (linear-linear)	−0.155	1.87	1.76	2321.7 2358.57	30.21 1.998241	4	114
3. $N_2H^+ + H$ (linear-atomic)	−2.535	0.97	0.67	3257.62* 698.64* 698.64* 2257.87*	1.55*	1	70.1

[a]References 3 and 31.

[b]The values marked * are taken from Ref. 30; the other values are from Ref. 35.

$$P_{(1)}(E,J)=\tilde{W}_3^{\ddagger}(E,J)\ \Big/\sum_i \tilde{W}_i^{\ddagger}(E,J), \tag{18}$$

$$P_{(2)}(E,J)=\tilde{W}_2^{\ddagger}(E,J)\ \Big/\sum_i \tilde{W}_i^{\ddagger}(E,J), \tag{19}$$

$$P_{(3)}(E,J)=\tilde{W}_3^{\ddagger}(E,J)\ \Big/\sum_i \tilde{W}_i^{\ddagger}(E,J), \tag{20}$$

$$P_{(4)}(E,J)=\tilde{W}_1^{\ddagger}(E,J)\ \Big/\sum_i \tilde{W}_i^{\ddagger}(E,J). \tag{21}$$

We see that the probabilities for reactions (1) and (3) are identical: this is because these reactions lead to the same product pair ($N_2H^+ + H$), and because for both reactions the same intermediate complex is supposed to form and decay. From these decay probabilities the reaction cross section $\sigma_i(E)$ for each of the processes is found by integrating over all values of J [as in Eq. (15)] with the weight function given by Eq. (16). This weight function depends on the input channel only (through μ and α). Adding the cross sections for all channels that are populated by the same input (reactant) channel gives the close collision cross section for the input channel considered: $\Sigma_i\sigma_i(E)=\sigma_{\mathrm{LGS}}$. Table II gives the close collision cross sections, calculated using Eq. (13) with $E_{\mathrm{kin}}=\frac{3}{2}\,kT$ and $T=300$ K.

In total, six reactions can be considered now: starting with $N_2^+ + H_2$, we can have formation of N_2H^+ according to (1), charge transfer according to (2), or we can have a backward reaction into the original reactant channel. Starting with $H_2^+ + N_2$, we can have three similar products: formation of N_2H^+ according to (3), charge transfer according to (4), and backward reaction. The calculated reaction cross sections as a function of the total energy available to the system are shown in Figs. 3 and 4 as solid curves. By scaling our experimental results to the theoretical curves, a calibration on an absolute scale was obtained (right hand vertical axes). In Fig. 3 we multiplied the calculated RRKM cross section for $N_2^+(A)$ by a factor of $\frac{1}{2}$, causing the discontinuity of the theoretical curve. This 50% reduction cannot be explained by RRKM theory alone and is explained in Sec. V below. Table II gives the data used in the RRKM calculations. In the calculations, we employed the so-called integral approximation of Ref. 29, which is suited for systems containing two linear molecules. The calculations were done at regular internal energy intervals of 100 meV.

For both atomic rearrangement processes, the calculated RRKM reaction cross section is almost independent of the internal energy of the reacting ion. Over a 3 eV range of internal energy we calculated a decrease of only 7% which is caused by increasing competition of the charge transfer and the backward channel, both being about equal in importance. This weak energy dependence is no surprise, since under all circumstances relevant for the present work, the $N_2H^+ + H$ channel is by far the most exothermal channel (see Table II), therefore having the largest phase space. This effect is even more pronounced because of symmetry. The symmetry species of N_2, N_2^+, H_2, and H_2^+ is $D_{\infty h}$, having rotational symmetry number $S=2$. This implies that the double-diatom channels $N_2^+ + H_2$ and $H_2^+ + N_2$ both have symmetry number equal to 4. The symmetry species of N_2H^+ is $C_{\infty v}$, having rotational symmetry number $S=1$. This is also the symmetry number for the $N_2H^+ + H$ channel. This implies that the $N_2H^+ + H$ channel has the lowest symmetry number, so that symmetry effects are in favor of this channel [see Eq. (14)]. This can be understood easily in a less formal language. After labeling the nuclei we can produce four forms of each channel by permutation of identical nuclei. For the $N_2H^+ + H$ channel, these forms cannot be transformed into each other by rotation (the N_2H^+ ion having the linear structure[30] NNH^+), and therefore are indeed different from each other. For the other channels these four forms are all related by rotation, and are essentially identical. This means that there are four transition states connected with the $N_2H^+ + H$ channel, whereas there is only one transition state connected with any other channel.

V. DISCUSSION

Comparing the calculated curves with the measurements, we see that for the $H_2^+ + N_2$ input channel, the theory correctly reproduces the experimentally observed behavior: a reaction cross section almost independent of internal energy and a negligible charge transfer cross section. For the $N_2^+ + H_2$ input channel, however, a discrepancy is found. The 50% decrease in reaction cross section that is observed experimentally when changing from $N_2^+(X)$ to $N_2^+(A)$ is not expected from RRKM theory, which predicts a cross section almost independent of internal energy, as we saw earlier. Charge transfer to $H_2^+ + N_2$ is correctly predicted by theory to be a process of minor importance.

To explain this discrepancy we present the following mechanism, based on a molecular orbital correlation diagram

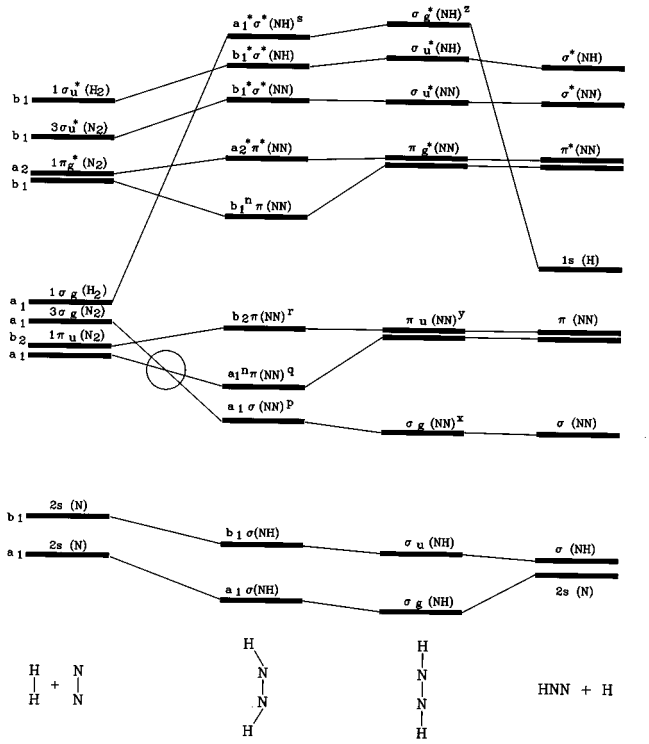

FIG. 5. Correlation diagram for the N_2-H_2 system. The reaction proceeds from left to right from separated reactants via the bent and the linear configuration of the HNNH nuclear skeleton into products, as indicated at the bottom of the figure. For the leftmost two columns, the electronic orbitals are labeled with the appropriate irreducible representation (a_1,a_2,b_1, or b_2) of the C_{2v} symmetry. One orbital crossing is indicated by a circle. For some orbitals, the population is denoted using the letters (p,q,r,s) and (x,y,z) (see text). Adapted from Refs. 31 and 33.

TABLE III. Evolution of the three experimentally investigated electronic states during the formation of the linear diimide ion $HNNH^+$. The rightmost column gives electronic configurations of this ion in order of increasing electronic energy. Of the $N_2^+(A)+H_2$ reactants, 50% evolve into (x,y,z) =(2,3,2), the same configuration that all $N_2^+(X)+H_2$ evolve into. The other 50% of the $N_2^+(A)+H_2$ evolve into (x,y,z)= (1,4,2), which has a higher electronic energy. The $H_2^+(X)+ N_2$ reactants all evolve into (x,y,z) =(2,4,1), which is the lowest state of the linear diimide ion that is found here.

Separated reactants ↓		Bent HNNH skeleton (p,q,r,s) ↓		Linear HNNH skeleton (x,y,z) ↓
$H_2^+(X,\ 1\sigma_g^{-1}) + N_2$	→	(2,2,2,1)	→	(2,4,1)
$N_2^+(X,\ 3\sigma_g^{-1})+H_2$	→	(2,1,2,2)	→	(2,3,2)
$N_2^+(A,1\pi_u^{-1})+H_2$	↗	(2,2,1,2)	→	(2,3,2)
	↘	(1,2,2,2)	→	(1,4,2)

that was first presented and discussed by Mahan (Ref. 31) and is shown here with some corrections[32] in Fig. 5. It was remarked by Mahan that the diimide ion, $HN{=}NH^+$, is a stable intermediate that can give rise to a persistent collision complex. To describe the reaction while it proceeds via this intermediate, a correlation diagram must be constructed for the approach of the two reaction partners which leads to one hydrogen atom on each side of the dinitrogen. This implies C_{2v} symmetry to be valid during the formation of the diimide ion. A reaction path in accordance with this symmetry is indicated below the diagram in Fig. 5. First, the separated reactants approach each other from infinite distance, with the N_2 and the H_2 molecule lying in the same plane, and with parallel internuclear axes (leftmost column). Next, the system passes through the bent and the linear configurations of the HNNH nuclear skeleton (middle two columns). Finally, it splits up into the products, having NNH and H nuclear skeletons (rightmost column). In the diagram, orbitals of the separated reactants and the bent HNNH nuclear skeleton are labeled with the appropriate irreducible representation (a_1, a_2, b_1, or b_2) of the C_{2v} symmetry. One crossing of orbitals having the same symmetry species (a_1) can be found and is indicated in the figure by a circle. Disregarding the four electrons in the $1s$ nitrogen atomic orbitals (these orbitals maintain their atomic character and are immaterial to our argument), we can now insert the remaining 11 electrons into the leftmost column of the diagram in three ways, according to the three different electronic configurations we investigated: $H_2^+(X,1\sigma_g^{-1})+N_2$, $N_2^+(X,3\sigma_g^{-1})+H_2$, and $N_2^+(A,1\pi_u^{-1})+H_2$.

For the description of the evolution of the electronic orbitals during the collision, we will use the following convenient shorthand notations:

$$(p,q,r,s)\equiv a_1\sigma(\mathrm{NN})^p\ a_1^n\pi(\mathrm{NN})^q\ b_2\pi(\mathrm{NN})^r\ a_1^*\sigma^*(\mathrm{NH})^s, \tag{22}$$

for the bent HNNH nuclear skeleton and

$$(x,y,z)\equiv\sigma_g(\mathrm{NN})^x\ \pi_u(\mathrm{NN})^y\ \sigma_g^*(\mathrm{NH})^z, \tag{23}$$

for the linear HNNH nuclear skeleton. The numbers (p,q,r,s) and (x,y,z) give the population of each individual electronic orbital. In Table III we give the evolution of the three different electronic configurations using this shorthand notation. For these evolutions, we assume that the indicated crossing of the two a_1 orbitals is avoided at all times, and that no radiationless transition from $N_2^+(A)$ to $N_2^+(X)$ occurs. In the table, two evolutions for $N_2^+(A)+H_2$ are given. As explained earlier, the electronic configuration of $N_2^+(A)$ is

$$(1\sigma_g1s)^2(1\sigma_u1s)^2(2\sigma_g2s)^2(2\sigma_u2s)^2(1\pi_u2p)^3(3\sigma_g2p)^2$$

with one of the $1\pi_u2p$ molecular orbitals occupied by two electrons and the other by a single electron. For isolated reactants, the two $1\pi_u$ molecular nitrogen MOs are completely degenerate. As can be seen from the correlation diagram, this degeneracy is removed during the formation of the diimide ion: the $1\pi_u(N_2)$ pair splits up into an a_1,b_2 pair of orbitals which are no longer equivalent to each other.[34] Switching over from $D_{\infty h}$ symmetry to C_{2v} symmetry, the

three $1\pi_u$ electrons of the $N_2^+(A)$ ion can evolve as $1\pi_u(N_2)^3 \rightarrow a_1^2 b_2$ or as $1\pi_u(N_2)^3 \rightarrow a_1 b_2^2$, with equal probabilities for each of the two possibilities, because initially the orbitals were degenerate. Therefore, we may expect that 50% of the $N_2^+(A)+H_2$ reacting systems evolves along the $a_1^2 b_2$ branch (third row in Table III), and the other 50 % along the $a_1 b_2^2$ branch (fourth row in Table III). The correlation diagram shows that the electronic energy for these two branches are far from comparable: the $a_1^2 b_2$ branch ends up in the $(x,y,z)=(2,3,2)$ configuration of the linear diimide ion, which is the same configuration the $N_2^+(X)+H_2$ reacting systems evolve into, whereas the $a_1 b_2^2$ branch ends up in the $(x,y,z)=(1,4,2)$ configuration, which obviously has a higher energy.

The rightmost column in Table III gives electronic configurations of the linear diimide ion in order of increasing electronic energy. All $H_2^+(X)+N_2$ reacting systems evolve into $(x,y,z)=(2,4,1)$, which is the lowest diimide ion state we can find here; all $N_2^+(X)+H_2$ reacting systems and 50% of the $N_2^+(A)+H_2$ reacting systems evolve into $(x,y,z)=(2,3,2)$, which has a higher electronic energy, and the other 50% of the $N_2^+(A)+H_2$ reacting systems evolve into $(x,y,z)=(1,4,2)$, which has the highest electronic energy. To explain our measurements, we postulate here that in the latter case the electronic energy is so high, that the product region cannot be reached anymore; i.e., we postulate the existence of a barrier in the potential energy hypersurface that cannot be neglected for 50% of the $N_2^+(A)+H_2$ reactant systems. For all other reacting systems, including the other 50% of the $N_2^+(A)+H_2$ reactant systems, the barrier is lower, and we postulate that it can be neglected in these cases, so that the loose transition states are rate-determining. (Of course, the argumentation given here is rather qualitative, and support from more detailed theoretical calculations is certainly desirable. However, such calculations clearly fall outside the scope of the present work.)

This mechanism predicts that exactly one half of the $N_2^+(A)+H_2$ systems reacts according to RRKM calculations, and that the other one half does not react at all but returns to the reactant region, thus remaining effectively unaltered. Therefore, the proposed mechanism is in complete accordance with our experimental results, showing a 50% decrease in reaction cross section going from $N_2^+(X)$ to $N_2^+(A)$ reactants. Figures 3 and 4 demonstrate this excellent agreement between theory and experiment, allowing calibration of our measured cross sections on an absolute scale (right hand vertical axes). Disregarding the very weak decrease of the RRKM cross sections, we find the following absolute cross sections for the rearrangement reactions. For reaction (1): $N_2^+ + H_2 \rightarrow N_2H^+ + H$, the cross section is $\sigma_{LGS} = 76.1$ Å^2 starting with $N_2^+(X;v=0,1)$, but it is $\frac{1}{2}\sigma_{LGS} = 38.05$ Å^2 starting with $N_2^+(A;v=0-5)$. For reaction (3): $H_2^+(X;v=0-6)+N_2 \rightarrow N_2H^+ + H$, the cross section is $\sigma_{LGS}=114$ Å^2.

VI. CONCLUSIONS

We reported measurements on the internal energy dependence of ion–molecule reactions and charge transfer in collisions of $N_2^+(X,A,B;v)+H_2$ and of $H_2^+(X)+N_2$ at thermal collision energies. We found that the reactive channel, producing N_2H^+, is the main product channel, and that charge transfer only plays a minor role. This agrees with the findings of other authors. The cross section for formation of N_2H^+ was found to be independent of the internal energy reactions in collisions of $H_2^+(X)+N_2$. For reactive collisions of $N_2^+(X,v)+H_2$ and of $N_2^+(A)+H_2$ the cross sections also seems to be independent of the vibrational energy, but not of the electronic state. Going from $N_2^+(X;v)$ to $N_2^+(A;v)$ the cross section decreases by 50%. We performed RRKM calculations on the system. The results confirm that reactive collisions are more important than charge transfer processes. Reactive collisions are predicted to be (almost) independent of internal energy over the energy range considered in this work. The 50% difference in reactive cross section between $N_2^+(X;v)$ and $N_2^+(A;v)$ could be explained using an electronic correlation diagram of the $(N_2–H_2)^+$ system. The doubly degenerate $1\pi_u 2p$ state of molecular nitrogen splits up into two nondegenerate states of the collision complex, the diimide ion. This implies that, during the collision, the $N_2^+(A;v)+H_2$ system can evolve in two different ways. We showed that one of these two possible electronic evolutions gives rise to a high barrier, inhibiting the reaction for 50% of the $N_2^+(A;v)+H_2$ systems.

Because of the excellent agreement between the present measurements and the statistical theory in combination with the electronic correlation diagram, we believe that the investigated systems behave statistically. This allows us to give the cross sections for the reactive collisions on an absolute scale. For reaction (1): $N_2^+ + H_2 \rightarrow N_2H^+ + H$, the cross section is $\sigma_{LGS}=76.1$ Å^2 starting with $N_2^+(X;v=0,1)$, but it is $\frac{1}{2}\sigma_{LGS}=38.05$ Å^2 starting with $N_2^+(A;v=0-5)$. For reaction (3): $H_2^+(X;v=0-6)+N_2 \rightarrow N_2H^+ + H$, the cross section is $\sigma_{LGS}=114$ Å^2. The charge transfer cross sections are at least one order of magnitude smaller.

It is important to note at this point that the inclusion of the $N_2^+(A;v)$ ions into the present thermal collision energy investigations provides qualitatively new experimental information on the $(N_2–H_2)^+$ system.

ACKNOWLEDGMENTS

We would like to express our gratitude towards Dr. H. Rudolph for his kind interest in this work and for his helpful discussions on the theoretical part of it. This work is part of the research program of the ''Stichting voor Fundamenteel Onderzoek der Materie (FOM)'' which is financially supported by the ''Nederlandse Organisatie voor Wetenschappelijk Onderzoek (NWO).''

[1] G. Herzberg, *Molecular Spectra and Molecular Structure I. Spectra of Diatomic Molecules* (Van Nostrand, Princeton, NJ, 1964).
[2] A. Lofthus and P. H. Krupenie, J. Phys. Chem. Ref. Data **6**, 113 (1977).
[3] S. L. Anderson, T. Turner, B. H. Mahan, and Y. T. Lee, J. Chem. Phys. **77**, 1842 (1982).
[4] G. Henri, M. Lavollée, O. Dutuit, J. B. Ozenne, P. M. Guyon, and E. A. Gislason. J. Chem. Phys. **88**, 6381 (1988).
[5] P. M. Hierl, L. W. Stratton, and J. R. Wyatt, Int. J. Mass Spectrom. Ion Proc. **10**, 385 (1972) as cited in Ref. 4.
[6] They could not distinguish N_2^+ and N_2H^+.

[7] R. H. Schultz and P. B. Armentrout, J. Chem. Phys. **96**, 1036 (1992).
[8] P. Tosi, O. Dmitrijev, and D. Bassi, J. Chem. Phys. **97**, 3333 (1992).
[9] I. Koyano, K. Tanaka, T. Kato, and S. Suzuki, Faraday Discuss. Chem. Soc. **84**, 265 (1987).
[10] D. Van Pijkeren, E. Boltjes, J. Van Eck, and A. Niehaus, Chem. Phys. **91**, 293 (1984).
[11] D. Van Pijkeren, J. Van Eck, and A. Niehaus, Chem. Phys. **103**, 383 (1986).
[12] C. E. Van der Meij, J. Van Eck, and A. Niehaus, Chem. Phys. **130**, 325 (1989).
[13] C. E. Van der Meij, Ph.D. thesis, Utrecht University, 1989.
[14] The adiabatic ionization potential is the minimum energy required to ionize a molecule to a specific electronic state.
[15] K. Kimura, S. Katsumata, Y. Achiba, T. Yamazaki, and S. Iwata, *Handbook of HeI Photoelectron Spectra of Fundamental Organic Molecules* (Japan Scientific Societies, Tokyo, 1981), and references therein.
[16] The internal energy dependent cross section for this reaction was measured earlier by Van Pijkeren *et al.* (Ref. 10). The present measurements on this reaction agree with the results of these authors.
[17] For H_2^+ there is competition between formation of $(H_2{-}N_2)^{+}*$ and formation of $(H_2{-}H_2)^{+}*$. One might suspect this competition to influence our results. This is not the case, however, since we are working under single-collision conditions, so that only a small fraction of the total H_2^+ is expected to form complexes anyhow, most of the H_2^+ simply not reacting at all.
[18] T. R. Govers, P. M. Guyon, T. Baer, K. Cole, H. Fröhlich, and M. Lavollée, Chem. Phys. **87**, 373 (1984).
[19] As is customary in spectroscopy, in the description of decay we will denote upper state vibrational quantum numbers with a single prime, and lower state ones with a double prime.
[20] D. C. Cartwright, J. Chem. Phys. **58**, 178 (1973) as cited in Ref. 18.
[21] In both Figs. 3 and 4 the horizontal axis gives the internal energy including $\frac{7}{2}kT \approx 91$ meV of thermal energy, consisting of a translational contribution of $\frac{3}{2}kT$ representing the center-of-mass collision energy plus a rotational contribution of kT for each of the two linear reactants.
[22] P. J. Robinson and K. A. Holbrook, *Unimolecular Reactions* (Wiley-Interscience, London, 1972).
[23] W. Forst, *Theory of Unimolecular Reactions* (Academic, New York, 1973).
[24] R. G. Gilbert and S. C. Smith, *Theory of Unimolecular and Recombination Reactions* (Blackwell, Oxford, 1990), and references therein.
[25] Quantum Chemistry Program Exchange, Program QCPE 557 TSTPST: Statistical Theory Package for RRKM/QET/TST/PST Calculations, QCPE Bulletin **8**, 137 (1988); code written by W. J. Chesnavich, L. Bass, M. E. Grice, K. Song, and D. A. Webb.
[26] M. P. Langevin, Ann. Chim. Phys. **5**, 245 (1905).
[27] G. Gioumousis and D. P. Stevenson, J. Chem. Phys. **29**, 294 (1958).
[28] W. J. Chesnavich and M. T. Bowers, J. Am. Chem. Soc. **98**, 8301 (1976), and references therein.
[29] M. E. Grice, K. Song, and W. J. Chesnavich, J. Phys. Chem. **90**, 3503 (1986), and references therein.
[30] J. C. Owrutsky, C. S. Gudeman, C. C. Martner, L. M. Tack, N. H. Rosenbaum, and R. J. Saykally, J. Chem. Phys. **84**, 605 (1986).
[31] B. H. Mahan, J. Chem. Phys. **55**, 1436 (1971).
[32] Mahan's original correlation diagram contains some errors. This was also remarked by Rose (Ref. 33), who gives another version of it, that still seems to contain some errors, however. The diagram presented here in Fig. 5 is a version of Mahan's original corrected by us.
[33] Ch. Rose, Ph.D. thesis MPQ 182, Max-Planck-Institut für Quantenoptik, Garching, Germany, 1993 (in German).
[34] In the proposed C_{2v} symmetry, but with the H_2 still far away, we can take one of the two π-orbitals to be lying in the plane containing the two internuclear axes, and the other one to be lying out-of-plane. The in-plane $1\pi_u 2p$ MO changes into a a_1 MO of the intermediate complex, and the out-of-plane $1\pi_u 2p$ MO into a b_2 MO.
[35] K. P. Huber and G. Herzberg, *Molecular Spectra and Molecular Structure IV. Constants of Diatomic Molecules* (Van Nostrand, Toronto, 1979).